An Overview of Computational Results at General Fusion Inc. with Focus on Hydrodynamics

Victoria Suponitsky, Sandra Barsky, Dustin Oliphant, and Peter Kostka

General Fusion Inc., 108-3680 Bonneville Place, Burnaby, BC V3N 4T5,Canada

Email: *victoria.suponitsky@generalfusion.com*

ABSTRACT

Fusion as a way to generate energy is currently undergoing a renaissance in scientific interest. The approach called Magnetized Target Fusion, a hybrid between magnetic fusion and inertial confinement fusion, is currently pursued by General Fusion. At General Fusion, our scheme is to inject plasma into an evacuated cylindrical cavity surrounded by rotating molten lead-lithium which is contained within a steel vessel, and then to compress it to thermonuclear conditions by a shock wave generated by pneumatic pistons placed on the vessel. This scheme was inspired from a project named 'LINUS', first developed by the US Naval Weapons Research Lab in Washington DC in the late 1970s.

Hydrodynamic aspects of the project include but are not limited to (i) designing a lead pumping scheme that assures formation of a stable cylindrical void cavity inside the vessel, and (ii) propagation of the pressure waves followed by the cavity collapse.

This overview describes the results of computational fluid dynamics (CFD) and finite element analysis (FEA) simulations that were carried out to deepen our understanding of mentioned above points (i) and (ii). Numerical results with regard to the cavity formation are qualitatively compared to our in-house experimental data, while for the pressure propagation and cavity collapse the results of CFD were compared to FEA simulations.

1 INTRODUCTION

Recently there has been a revival of interest in controlled fusion as a source of energy. A number of projects worldwide, from both public and private industry, are currently examining ways to create a commercial source of fusion energy. The approach pursued by General Fusion is first to merge two hydrogen spheromaks inside the central evacuated cavity surrounded by molten lead-lithium (PbLi) and then to sufficiently compress the spheromaks by pressure waves in order to satisfy thermonuclear conditions and obtain fusion. A cavity is formed as a result of tangential pumping of PbLi into a vessel having a drainage hole on the bottom. The pressure waves are initiated by striking the outer surface of the PbLi with pneumatic steel pistons. The amplitude of the pressure waves and shape of the wave front in proximity of the lead-lithium/vacuum interface are determined by initial velocity of the pistons, their arrangement at the surface of the vessel and time of firing. Geometry and size of the piston also influence the shape and strength of the pressure wave resulting from the impact.

In a first step towards our final goal, we are in the process of constructing a prototype sphere consisting of a small steel spherical vessel with two rings of pistons. The sphere is $1m$ in diameter and the rings consist of 7 pistons each and are symmetrically placed on either side of the equator, Fig. 1. The working fluid is lead (Pb). The piston assemblies consist of an outer piston which is accelerated by compressed air, and an inner piston which directly contacts the lead. The pistons are placed so that in the case of simultaneous firing the convergent focal point is the center of the sphere.

We report here on simulations done during the design stages of the prototype. The rest of the paper is organized as follows: Section 2 describes results of the cavity/air-core formation simulations which were carried out for both water and lead. The results of the water simulations were then compared to in-house experimental data. Section 3 deals with (i) pressure waves propagation in the vessel, pistons and liquid lead, and (ii) air/vacuum cavity collapse.

2 AIR-CORE FORMATION

The results presented in this section were obtained using the open source CFD code OpenFOAM [1]. The incompressible multiphase solver 'interFoam' was

used in these simulations. This solver implements the Volume Fraction (VOF) method for interface tracking and is suitable for the simulation of two immiscible isothermal fluids. Full $3D$ transient simulations were carried on a computational mesh having approximately 2 million grid points.

Our CFD computational model consists of a sphere with two drainage pipes open to the atmosphere at the top and bottom of the sphere, *i.e.* north and south poles. Liquid is pumped nearly tangentially into the sphere through a number of pumping nozzles located either near the bottom of the sphere, Fig. 2a, or at the equator, Fig. 2b. The injection flow rate was approximately $\dot{q} = 0.007 m^3/s$, which corresponds to the nominal flow rate used in our experiments. The setup used in our water sphere experiments is shown in Fig. 3. Simulations were carried for two sets of parameters: (i) diameter of the sphere $D_{sphere} = 1m$ and diameter of the drainage $d_{drain} = 0.1m$, and (ii) $D_{sphere} = 0.8m$ and $d_{drain} = 0.065m$. The former geometry corresponds to the prototype under construction, and the latter to the in-house water sphere experiment. Simulations were carried out for different sizes and number of the pumping nozzles. Between two and eight nozzles were used, and the nozzle size varied between $2.54cm \leq d_{pump} \leq 5.08cm$. Simulations were performed for both water ($\rho_{water} = 1000kg/m^3$, $\nu_{water} = 1 \times 10^{-6} m^2/s$, $\sigma_{water} = 0.07N/m$) and lead ($\rho_{lead} = 10000kg/m^3$, $\nu_{lead} = 1.38 \times 10^{-7} m^2/s$, $\sigma_{lead} = 0.44N/m$). It is worth noting that a real reactor is designed to operate in vacuum, such that the air-core will be replaced by a vacuum-core. We expect however, that with respect to hydrodynamics, this will have little effect on the formation mechanism. Initially the sphere was filled with air such that an entire process of filling followed by the air-core formation was simulated.

A typical process of air-core vortex formation is shown in Fig. 4. Results are shown for the case of equatorial injection with the seven pumping nozzles having a diameter of $d_{pump} = 2.54cm$. The total flow rate is $\dot{q} = 0.007 m^3/s$. For a given set of parameters a sphere is expected to be filled within $T_{filling} \approx 75s$ when the drainage hole is closed. During the filling process, Fig. 4(a)-Fig. 4(c), the air originally residing in the sphere gets pushed out mostly through the upper drainage hole. The air inside the sphere is rotated by the swirling water and its rotation intensifies as the filling process goes on and the volume of the air inside the sphere goes down. Fig. 4(d) shows that once the system reaches its steady state a cylindrical air-core spanning the entire height of the sphere and strongly communicating with an outside atmosphere is formed. At this point it is important to reiterate, the main goal of this part of the project is to demonstrate that we are able to provide a pumping system along with a range of parameters under which a stable air-core is formed when the system reaches its steady state. With this in mind it is of interest to compare the flow characteristics at the latest stages of filling Fig. 4(c), with those when flow settles into an equilibrium state Fig. 4(d), since the shape of the volume occupied by the gas is not too different. One can see that near the liquid-gas interface both the rotational and vertical velocities are significantly higher for the flow in equilibrium. There is also evidence of air flow inside the core due to its communication with the surrounding atmosphere when the steady state has been reached.

It is important to note that during the filling of the sphere the system is open, *i.e.* there is no strong coupling between the injected and drained fluid. Angular momentum accumulates inside the sphere and is equal to the total angular momentum injected into the sphere minus angular momentum taken away by the drained fluid, which is driven solely by gravity. Once the sphere is completely filled the system becomes a closed one, *i.e.* there is a strong coupling between the input (injection) and output (drainage) of the system. Once in equilibrium, all angular momentum further added to the system by the injection needs to be taken out of the system by the draining fluid, so that angular momentum inside the sphere remains constant. This explains a sudden increase in the rotational velocity at radial distances comparable with the radius of the drainage once the system reaches equilibrium, as now the fluid has to leave the sphere with significantly higher angular momentum. Due to the sudden increase of rotation, the pressure in the center of the sphere decreases. This is likely to be a reason for the air-core formation, *i.e.* the air from the surrounding atmosphere is sucked into the sphere due to the developed pressure gradient which in turn often results in the formation of a reasonably stable air-core. It is also worth noting that once pumping is turned off the system immediately switches back to the open state which is accompanied by a sudden decrease in the rotating velocity component. This sudden change in rotation is also clearly seen in our experiments by the abrupt change in the cone angle of the fluid leaving the drainage hole.

The cylindrical air-core formation obtained in simulations is qualitatively similar to the one observed in our water sphere experiments: (i) when the injection parameters are such that we were able to fill in the sphere completely, a nearly cylindrical air-core has been always formed, (ii) formation process of this cylindrical air-core is a sudden and violent event:

sometimes the existing gas region almost completely disappears before a cylindrical air-core is formed by sucking the air from the surrounding atmosphere, (iii) rotational velocity of the water-air interface is much higher for the cylindrical air-core vortex formed once the sphere is completely filled, when compared to the slightly tapered air-core observed during the latest stages of the filling process.

Once a cylindrical air-core was formed, the numerical data was accumulated over the next 10*s* to obtain time-averaged structure of the flow field. Contours of the mean vertical velocity and its profile close to the bottom drainage hole ($Z = -0.4m$) are shown in Figs. 5(a) and (b), respectively. Near both drainage holes a vertical velocity field illustrates the phenomena of bidirectional vortex, *i.e.* existence of the thin layer inside which a translatory component of the spiral motion changes its direction,e.g. [3]. The strongest velocity gradients across this layer occur in close proximity of the drainage holes.

Radial profiles of rotational velocity and pressure in the equatorial plane are shown in Figs. 6(a) and (b), respectively. Results with the bottom injection are shown for both water and lead. As expected, the overall vortex structure is a combination of viscous core (forced vortex which is characterized by a nearly constant shear) in the center of the sphere and a free potential vortex away from the center. The central part of the viscous core is occupied by an air-core, and its diameter is obtained from the field of volume fraction. The location of the gas-liquid interface can be also identified by a small wiggle in the velocity profile. Shear stresses should be equal on the both sides of the liquid-gas interface therefore the velocity gradient is discontinuous across the interface between fluids with different viscosity.

The overall structure of the flow field in our simulations is very similar to the one often occurring inside hydrocyclones, e.g. [4]. The mechanism of the air-core formation observed in hydrocyclones is of practical importance, as it significantly affects the efficiency of the hydrocyclone. This recently prompted a number of studies on the subject with an ultimate goal of suppressing the air-core formation [6, 7, 8, 9, 10].

The main goal of water sphere experiments and numerical simulations is to get a feeling for the parameters required to recreate a similar gas cavity in the reactor prototype (argon-core within liquid lead). Comparing the results for water and lead one can see that the difference in Reynolds number and surface tension have very little effect on the velocity profile, but a radial pressure at the wall of the sphere is an order of magnitude higher for the lead. The radial pressure distribution can be estimated as $P(r) = \rho \cdot \int_0^r v_\theta^2/r\, dr$, therefore for the similar velocity distribution the pressure scales with density. The density of lead is 10 times more than the density of water, therefore the increase of an order of magnitude in the pressure is exactly what we expect to get, providing nearly the same velocity profiles. Comparison between velocities measured in experiments with those obtained in simulations showed a consistent significant overestimation of maximum velocity in the simulations. This is not uncommon, analytical models and numerical simulations are tend to overestimate maximum velocity, e.g. [5, 11].

Fig. 7 shows rotational velocity and pressure for simulations with equatorial injection. For the same flow rate and injection geometry, a decrease in the size of pumping nozzles leads to increase of the injection velocity. This means that a decrease in the nozzle size leads to an increase of the angular momentum injected into the system, which in turns results in an increase of the maximum rotational velocity. Fig. 7 also shows that for higher equatorial injection velocities, velocity does not decay as $1/r$ far from the center, but stays flat; this has also been observed in experiments. Moreover, in the experiments with high equatorial injection velocities, the system was not able to stay in an equilibrium for long: an initially stable air-core began to precess. The cylindrical air-core is getting distorted and replaced by a rather violently spinning tapered vortex. Simulations for similar cases also show development of instabilities leading to the precessing of the air-core. One explanation for this phenomenon is that with high injection velocities too much angular momentum is injected into the system. This leads to the high rotational velocity which in turn leads to increase in diameter of the vortex core. With the increase in the size of the air-core there is less and less space available for liquid to drain out of the sphere. This carries on until air-core is finally pushed away from the drainage hole to allow liquid easier escape from the sphere.

3 PRESSURE WAVES

Both CFD and FEA simulations were carried out to study pressure waves propagation inside the lead. The pressure waves travel at the speed of sound in lead $\approx 1800m/s$; since this is so much greater than the rotational velocity $\approx 10m/s$ the rotation of the fluid is not taken into account for this part of the study. In these simulations, the cylindrical core of air in the CFD simulations and vacuum in the FEA is artificially imposed at the centre. The pressure gradients developing in the lead as a result of fluid rotation are also not taken into account. We expect this to have little effect on the results as the increase in the pressure due to rotation is of

order of $10atm$, whereas the amplitude of the pressure waves initiated by the impact of the pistons is of order $10000atm$.

The FEA analysis was done using commercial package LS-Dyna [2]. The computational model used in FEA simulations is shown in Fig. 8. The model consists of steel pistons and a steel spherical vessel occupied by liquid lead with a cylindrical vacuum in the interior. For steel parts a standard Lagrangian mesh was used, whereas the lead and the vacuum were modeled with Eulerian elements. The steel and lead were coupled through fluid-structure interaction parameters. The outer piston was given an initial velocity of $50m/s$. It strikes the inner piston, creating a pressure wave which then travels through the inner piston to strike the lead. Fig. 9 shows a typical cross-section pressure distribution obtained in the simulations of an isolated piston. One can see that the pressure is greatest at the center and decreases towards the edges. This is due, in part, to the geometry of the piston. The initial pressure across the face is uniform, but the cylindrical sides of the piston expand and then contract back to regain their equilibrium, *i.e.* zero stress, state. This contraction sends a wave back to the center of the piston, thereby concentrating the pressure at the center of the piston.
The pressure wave created by the impact of the piston on lead is shown in Fig. 10. As the waves travel toward the center of the sphere, waves from the different pistons merge creating a region of high pressure at the center of the sphere. A snapshot of the pressure profile just before the vacuum cavity is impacted is shown in Fig. 11. The interaction between the pressure in the lead and in the steel is also evident from the figure: the pressure imparted by the impact of the piston expands in a hemispherical manner in the lead.
In CFD simulations fluid-structure interaction between steel and lead was omitted completely, such that only pressure waves through the lead were considered. Piston impact was imposed through time-dependent pressure boundary condition applied at the surface of the sphere covered by the pistons. Impact pressure profile was roughly taken from FEA simulations; pulse duration is $T_{pulse} = 1 \times 10^{-4}s$ and maximum amplitude is $P_{max} = 1.4GPa$. Currently the uniform pressure across the entire piston face was prescribed. Pressure waves propagation in the lead obtained in CFD simulations is shown in Fig. 12. The main differences between FEA and CFD simulations setups are: (i) In CFD, the steel sphere is treated as a rigid boundary, i.e. there is no energy transfer between lead and steel. The pressure waves are dissipated in CFD simulations only through the viscous mechanism. In FEA simulations both elastic and plastic response are modeled. This results in higher amplitude of the pressure waves inside the lead and also a more regular wave pattern in the CFD simulation; (ii) Uniform pressure distribution across face of the piston in the CFD simulations. This leads to the higher pressures predicted by CFD in particular near the poles of the sphere; (iii) Central cylindrical cavity is filled with air in CFD simulations as opposed to vacuum in FEA. This affects the later stages of the collapse, as air is going to push back on lead.
The above differences between FEA and CFD simulations had a significant effect on the collapse of the cavity: in FEA simulations the cavity has always collapsed first in the middle of the sphere, whereas CFD simulations consistently showed so called pinch-like collapse, where the cavity first collapses close to the poles and later in the middle. A physical mechanism of the cavity collapse is a very complex phenomenon that deserves a separate investigation, the results of which will be reported elsewhere. In a nutshell, the discrepancy between FEA and CFD results can be explained by stronger pressure waves occurring near the poles of the sphere in CFD simulations as a result of different the initial setups.

ACKNOWLEDGMENTS

We would like to thank Dr Aaron Froese and Dr Meritt Reynolds for their highly valuable input during our never ending discussions concerning vortex formation and pressure wave propagation mechanisms.

REFERENCES

[1] OpenFOAM. www.openfoam.org.

[2] LS-Dyna www.ls-dyna.com.

[3] J. Majdalani and S.W. Rienstra On the bidirectional vortex and other similarity solutions in spherical coordinates. *ZEITSCHRIFT FUR ANGEWANDTE MATHEMATIK UND PHYSIK (ZAMP)*, 58(2):289–308, 2007.

[4] R. Gupta and M.D. Kaulaskar and V. Kumar and R. Sripriya and B.C. Meikap and S. Chakraborty. Studies on the understanding mechanism of air core vortex formation in a hydrocyclone. *Chemical Engineering Journal*, 144:153-166, 2008.

[5] B.A. Maicke and J. Majdalani A constant shear stress core flow model of the bidirectional vortex *Proc. R. Soc. A*, 465:915-935, 2009.

[6] T. Dyakowski and R.A. Williams. Prediction of air-core size and shape in a hydrocyclone. *Int. J. Miner. Process.*, 43:1-14, 1995.

[7] T. Neesse and J. Dueck. Air core formation in the hydrocyclone. *Minerals Engineering*, 20:349-354, 2007.

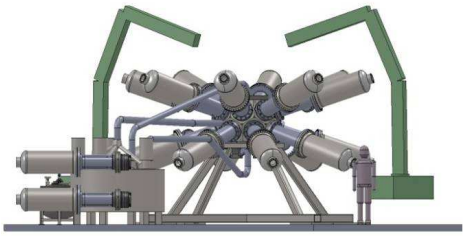

Figure 1: A schematic of the prototype which is currently under construction in General Fusion.

[8] B. Wang and K. W. Chu and A. B. Yu. Numerical Study of Particle - Fluid Flow in a Hydrocyclone. *Ind. Eng. Chem. Res.*, 46:4695-4705, 2007.

[9] M. Narasimha and M. Brennan and P. N. Holtham. Large eddy simulation of hydrocyclone-prediction of air-core diameter and shape. *Int. J. Miner. Process.*, 80:1-14, 2006.

[10] S. Kim and T. Khil and D. Kim and Y. Yoon. Effect of geometric parameters on the liquid film thickness and air core formation in a swirl injector. *Meas. Sci. Technol.*, 20:015403, 2008.

[11] A. Skerlavaj and A. Lipej and J. Ravnik and L. Skerget. Turbulence model comparison for a surface vortex simulation. *25th IAHR Symposium on Hydraulic Machinery and Systems*,12,2010.

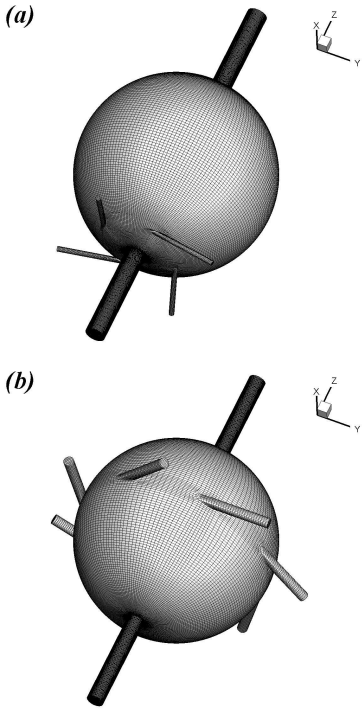

Figure 2: Computational model used in the air-core vortex generation simulations. (a) bottom injection; (b) equatorial injection.

Figure 3: Setup for the in-house water sphere experiment. With configuration shown water is injected through the four pumping nozzles located near the equator. With current set of parameters a sphere appears to be completely filled with water and a stable cylindrical air-core spanning entire height of the sphere is clearly seen.

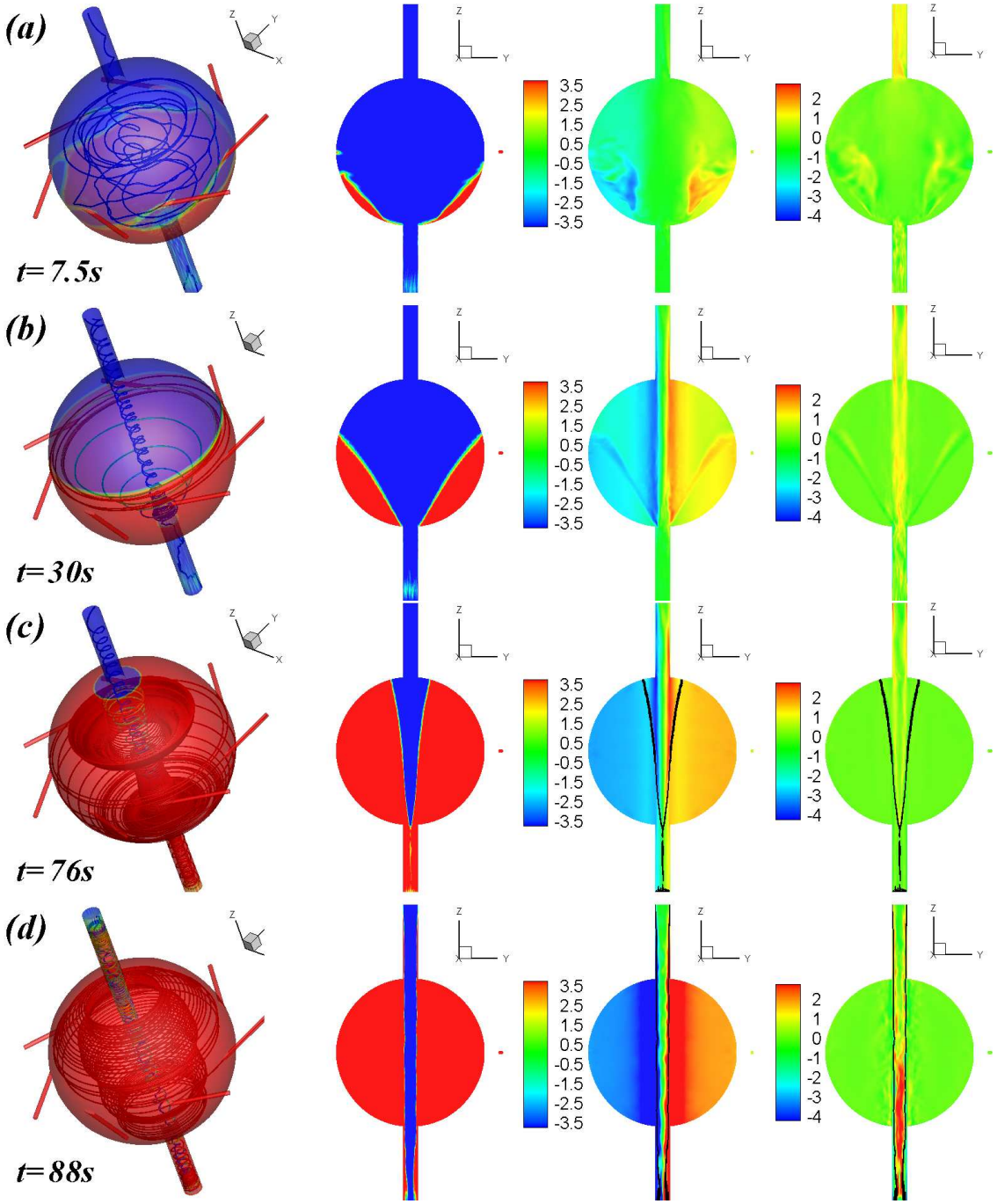

Figure 4: Air-core vortex formation process; parts (a)-(d) correspond to different times during the formation process. First column: streamlines; second column: volume fraction (red - water, blue - air); third column: swirl velocity (corresponds to the x- velocity component for the cross-section presented); forth column: vertical velocity (z-velocity component). ($D_{sphere} = 1m$, $d_{drain} = 0.1m$, $d_{pump} = 2.54cm$, $\dot{q}_{total} = 0.007m^3/s$)

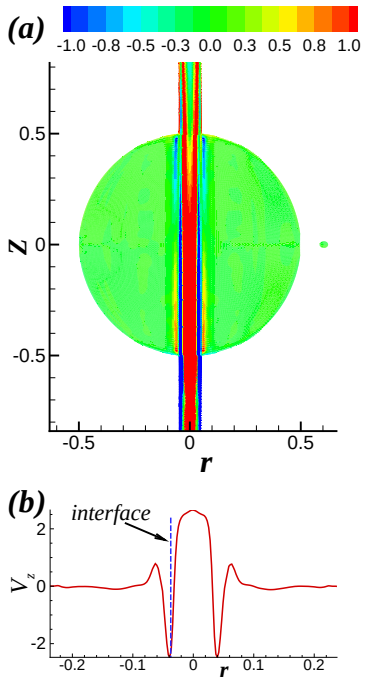

Figure 5: (a) Mean vertical (V_z) velocity contours at $X = 0$ cross-section; (b) Vertical velocity profile at $Z = -0.4m$.

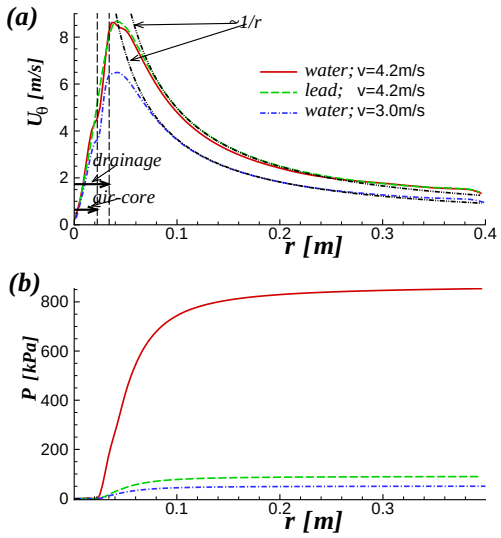

Figure 6: Lead .vs water; (a) Average swirling velocity profile at $Z = 0$; (b) Radial pressure distribution at $Z = 0$. Results are shown for the case of bottom injection with four pumping nozzles; $\dot{q} = 0.01m^3/s$ for $v_{injection} = 4.2m/s$; $\dot{q} = 0.00785m^3/s$ for $v_{injection} = 3m/s$, $D_{sphere} = 0.8m$.

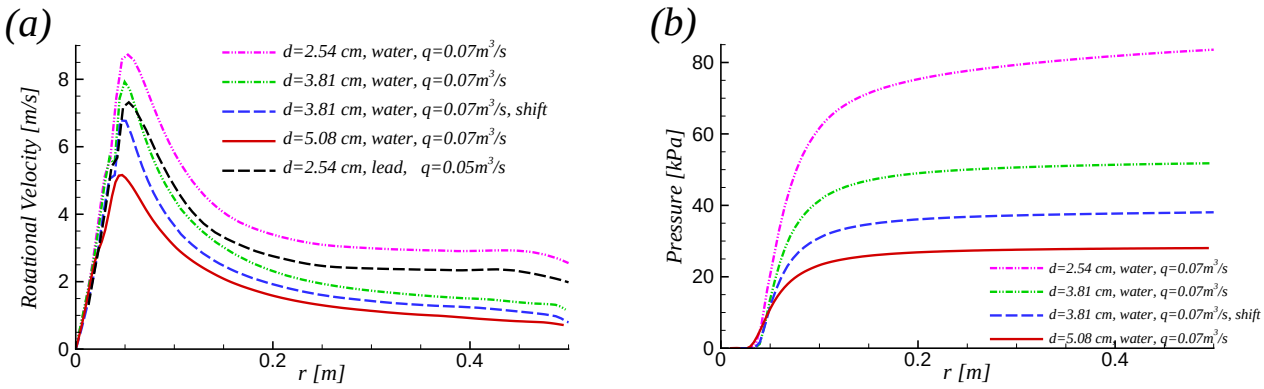

Figure 7: Typical average profiles at $Z = 0$ of (a) swirling velocity and (b) pressure. Results are shown for the sphere with $D_{sphere} = 1m$ and seven pumping nozzle at the equator. Results are shown for different sizes of the pumping nozzles and different flow rates (as indicated in the legend). 'shift' in the legend indicates that the pumping direction was slightly shifted from being tangential. In this case the pumping nozzle was shifted towards the center by $6.35cm$.

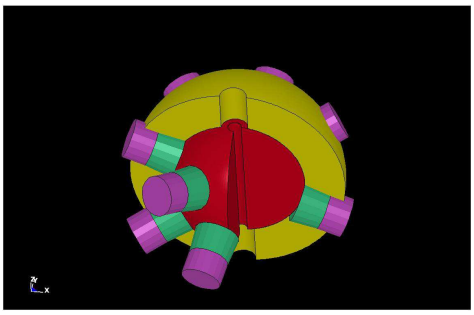

Figure 8: A view of the sphere used in the LS-Dyna calculations. The interior of the sphere, in red, is lead. It is surrounded by a 30 cm casing of steel. Some of the 14 pistons are shown. The piston surface in contact with the lead is curved to maintain a spherical shape. The vacuum mesh is not shown, thus the hole through the center of the sphere is the vortex created by spinning fluid.

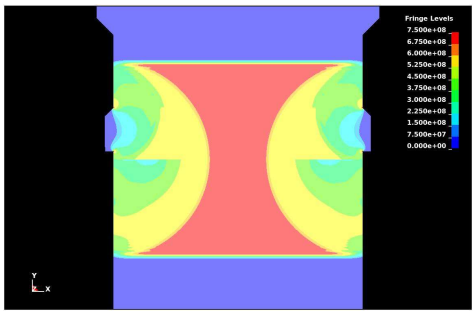

Figure 9: A cross-sectional view of the pressure profile through both pistons. The delimiting edge of the pistons is approximately halfway through the view, where the pressure is discontinuous. (In this simulation of the isolated piston the computational mesh was finer than that used in full 3*D* piston-sphere simulations.)

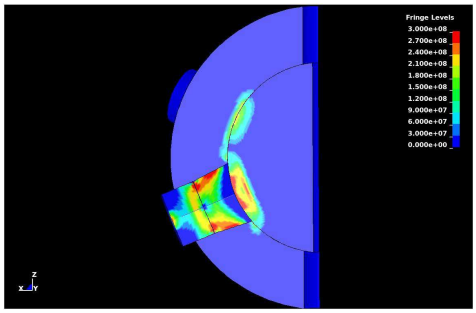

Figure 10: The pressure created from impacting steel pistons traveling into the lead. The pressure from distant pistons is also seen.

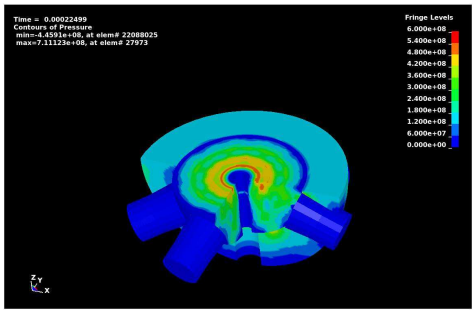

Figure 11: An equatorial view of the pressure in the lead just before it impacts the vortex. The pressure waves created from the individual pistons have merged to create a uniform pressure wave at the center of the sphere. One can also see in this picture how the lead and steel interact. Near the south pole, pressure is leaking from the lead into the steel.

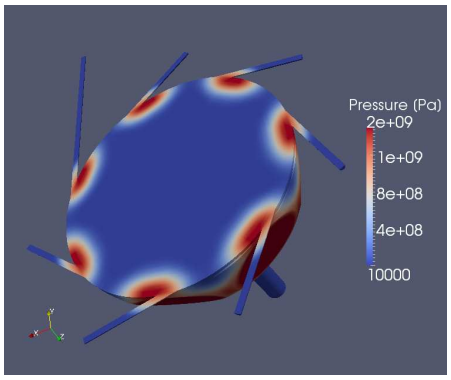

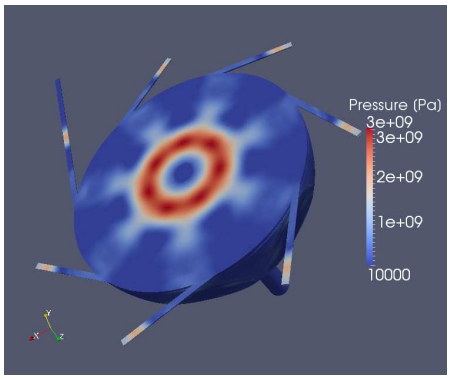

Figure 12: Propagation of the pressure waves inside the lead obtained in CFD simulations; just after the piston impact (left) and before hitting liquid-gas interface (right).